JOURNAL OF ENVIRONMENTAL SCIENCES 74 (2018) 116–125

Available online at www.sciencedirect.com

ScienceDirect

www.elsevier.com/locate/jes

JES JOURNAL OF ENVIRONMENTAL SCIENCES

www.jesc.ac.cn

Fluorescence regional integration and differential fluorescence spectroscopy for analysis of structural characteristics and proton binding properties of fulvic acid sub-fractions

Fanhao Song[1], *Fengchang Wu*[1,*], *Weiying Feng*[1], *Zhi Tang*[1], *John P. Giesy*[1,2], *Fei Guo*[1], *Di Shi*[1], *Xiaofei Liu*[3], *Ning Qin*[1], *Baoshan Xing*[4], *Yingchen Bai*[1,*]

1. *State Key Laboratory of Environmental Criteria and Risk Assessment, Chinese Research Academy of Environmental Science, Beijing 10012, China*
2. *Department of Biomedical and Veterinary Biosciences and Toxicology Centre, University of Saskatchewan, Saskatoon, Saskatchewan, SK S7N 5B3, Canada*
3. *College of Resources, Environment and Tourism, Capital Normal University, Beijing 100048, China*
4. *Stockbridge School of Agriculture, University of Massachusetts, Amherst, MA 01003, USA*

ARTICLE INFO

Article history:
Received 6 December 2017
Revised 24 February 2018
Accepted 26 February 2018
Available online 3 March 2018

Keywords:
Fluorescence titration
Protonation
Modified Stern-Volmer equation
Dissociation constant
Binding

ABSTRACT

Structural characteristics and proton binding properties of sub-fractions (FA_3–FA_{13}) of fulvic acid (FA), eluted stepwise by pyrophosphate buffer were examined by use of fluorescence titration combined with fluorescence regional integration (FRI) and differential fluorescence spectroscopy (DFS). Humic-like (H-L) and fulvic-like (F-L) materials, which accounted for more than 80% of fluorescence response, were dominant in five sub-fractions of FA. Based on FRI analysis, except the response of F-L materials in FA_9 and FA_{13}, maximum changes in percent fluorescence response were less than 10% as pH was increased from 2.5 to 11.5. Contents of carboxylic and phenolic groups were compared for fluorescence peaks of FA sub-fractions based on pH-dependent fluorescence derived from DFS. Static quenching was the dominant mechanism for binding of protons by FA sub-fractions. Dissociation constants (pKa) were calculated by use of results of DFS and the modified Stern-Volmer relationship. The pK_a of H-L, F-L, tryptophan-like and tyrosine-like materials of FA sub-fractions exhibited ranges of 3.17–4.06, 3.12–3.97, 4.14–4.45 and 4.25–4.76, respectively, for acidic pHs. At basic pHs, values of pKa for corresponding materials were in ranges of 9.71–10.24, 9.62–10.99, 9.67–10.31 and 9.33–10.28, respectively. At acidic pH, protein-like (P-L) materials had greater affinities for protons than did either H-L or F-L materials. The di-carboxylic and phenolic groups were likely predominant sites of protonation for both H-L and F-L materials at both acidic and basic pHs. Amino acid groups were significant factors during proton binding to protein-like materials of FA sub-fractions at basic pH.

* *Corresponding authors. E-mails:* wufengchang@vip.skleg.cn (Fengchang Wu), yingchenbai@163.com (Yingchen Bai).

https://doi.org/10.1016/j.jes.2018.02.015
1001-0742/

Introduction

Fulvic acids (FA) comprize the main mobile fraction of dissolved organic matter (DOM), which can control speciation and mobilization of metals, organic chemicals and other environmental contaminants (Giesy, 1983; Giesy et al., 1986; Maqbool and Hur, 2016; Wang et al., 2016; Yamashita and Jaffé, 2008). In aquatic systems, increasing or decreasing pH can affect interactions between FA and various chemical species, especially metal ions (Alberts and Giesy, 1983; Giesy et al., 1978; Su et al., 2016; Yan et al., 2013; Zhang et al., 2010). In addition, pH can also influence sizes and optical properties of FA (De Haan et al., 1983; Lochmueller and Saavedra, 1986; Timko et al., 2015; Yan et al., 2013). Due to expansion of molecular structures or incorporation of new molecules into the aggregate, increasing pH resulted in an increase in molecular sizes of FA (De Haan et al., 1983; Lochmueller and Saavedra, 1986). Due to protonation and deprotonation of carboxylic-like and phenolic-like chromophores, distinguished by fluorescence parallel factor analysis, fluorescence of Suwannee River FA increased and decreased with pH decreasing or increasing, respectively (Yan et al., 2013). However, because of the extreme heterogeneity of FA, influences of pH on environmental behaviors of FAs have not been fully characterized.

Three-dimensional excitation-emission matrix (EEM) has proved to be a sensitive, selective, non-destructive method to characterize and quantify binding of DOM with protons and/or metal ions (He et al., 2014; Wu et al., 2011). Fluorescence regional integration (FRI) is a quantitative technique used to integrate areas beneath, operationally defined, EEM regions and analyze wavelength-dependent fluorescence of EEMs (Chai et al., 2012; Chen et al., 2003; Sun et al., 2016). FRI could provide information about relative compositions of various DOM, which had been derived from various environments, including soils, landfill leachates, bioreactors, and drinking waters (He et al., 2011; Massicotte and Frenette, 2011; Wu et al., 2012; Zhou et al., 2013). A more recent method that has proven to have advantages for elucidating properties of DOM, is differential fluorescence spectroscopy (DFS), which has eliminated fluorescence of non-reactive matter and allows examination of subtle changes in EEMs compared to traditional "peak picking" methods (Yan et al., 2013). Recently, DFS was successfully employed to estimate effects of pH on fluorescence of natural organic matters isolated from the Suwannee River and a Nordic Reservoir (Yan et al., 2013). However, as a new method, DFS had not been utilized to characterize binding of protons with sub-fractions of FA.

Dissociation constants (K_a), based on pH-dependent fluorescence in an acidic pH range (1.0–5.0), have been used to characterize DOM isolated from marine and stream water (Midorikawa and Tanoue, 1998; Wu and Tanoue, 2001). However, mechanisms for quenching of fluorescence or absence of measurable K_a of DOM with protons had not yet been systematically investigated at basic pHs. The Scatchard function has been used extensively to identify the type of binding and the number of sites (Giesy et al., 1986; Giesy and Alberts, 1982; Scatchard, 1949). Like Scatchard plot, the Eadies double-reciprocal plot were also widely used to isolate the parameters and fit the metal binding data and interpret the results without the need to fit four non-independent parameters (Giesy et al., 1986; Giesy and Alberts, 1989). In addition, a modified Stern-Volmer equation has been commonly employed to determine mechanisms for quenching of fluorescence, including dynamic and static quenching, and binding parameters by fitting changes in intensities of fluorescence of two-dimensional fluorescence spectra or EEM upon the addition of metal ions (Berkovic et al., 2012; Esteves da Silva et al., 1998; Lu and Jaffe, 2001). In the study, results of which are presented here, possible mechanisms of quenching of fluorescence of DOM by protons were confirmed by (a) exploring the curvature with a modified Stern-Volmer plot and (b) comparing association constants with an efficient quencher (Wu et al., 2013). Both DFS and the modified Stern-Volmer were related to differences of fluorescence spectra observed during fluorescence titration (Yan et al., 2013). To our knowledge, the modified Stern-Volmer equation has not been used previously to establish the K_a between DOM and proton at acidic and basic pH ranges.

Techniques for fractionating FA into sub-fractions by use of stepwise elution from XAD-8 with pyrophosphate buffers have been developed to reduce complexities of mixtures of FA (Bai et al., 2015). In this study, five sub-fractions of FA were used as follows: (1) to characterize differences in structures among sub-fractions of FA by use of FRI analysis; (2) to identify mechanisms of pH-depended changes in fluorescence; (3) to calculate pK_as of FA sub-fractions by use of DFS combined with use of a modified Stern-Volmer equation.

1. Materials and methods

1.1. *Sample pretreatment and fluorescence titration*

Methods for collection of samples and sequential fractionating of FA sub-fractions have been reported elsewhere (Bai et al., 2015). In brief, samples were collected at a depth of 0–15 cm from the Jiufeng Mountain Forest, Beijing, China. The soil samples were air-dried, ground to pass through the mesh and stored at 15°C before analyses. The Chinese standard FA was extracted from soil samples according the detailed procedures recommended by the International Humic Substances Society (IHSS, http://humic-substances.org). The purifications of FA were performed using the treatment of hydrogen fluoride combined with the XAD-8 resin and H^+-saturated cation exchanged resin techniques (Bio-Rad, Richmond, CA). The purified and freeze-dried FA was sequentially separated into five sub-fractions of FA named as FA_3, FA_5, FA_7, FA_9, and FA_{13} by use of the XAD-8 resin coupled with pyrophosphate buffers with pHs of 3.0, 5.0, 7.0, 9.0 or 13.0, respectively (Bai et al., 2015; Song et al., 2017, 2018). All sub-fractions of FA were re-purified by loading them onto an H^+-saturated cation exchanged resin (Bio-Rad, Richmond, CA). Finally, all sub-fractions of FA were lyophilized and stored for analysis (Bai et al., 2015).

During fluorescence titrations, solutions of sub-fractions of FA were prepared at 10.0 mg/L, and background ionic strength of solutions were established by including 0.05 mol/L $KClO_4$ as a background electrolyte. pHs of solutions were controlled by injecting sub-microliter amounts of $HClO_4$ or KOH to derive

values of 2.5 to 11.5 and kept under nitrogen for 15 min to allow equilibration. All chemicals used were analytical reagent grade unless otherwise specified. All solutions were prepared in Milli-Q water and filtered through 0.45-μm glass fiber membrane filters (Whatman, UK) before use.

1.2. Fluorescence spectroscopy

A fluorescence spectrometer (Hitachi F-7000, Tokyo, Japan) was used, at room temperature, to measure EEMs of FA sub-fractions. Excitation wavelength (Ex), emission wavelength (Em), scan speed and slit widths were reported previously (Song et al., 2017). EEMs of the $KClO_4$ blank were subtracted from EEMs of FA fractions. Interpolation was used to regulate the Rayleigh and Raman scatters (Murphy et al., 2013; Stedmon and Bro, 2008; Yu et al., 2010).

1.3. FRI analysis

In the FRI method, each EEM was divided into five regions (Regions I–V), using consistent Ex and Em boundaries (Chen et al., 2003; He et al., 2013; Sun et al., 2016). FRI parameters of percent fluorescence response ($P_{i,n}$, %) were calculated (Eq. (1)).

$$P_{i,n} = \frac{\varnothing_{i,n}}{\varnothing_{T,n}} \times 100\% = \frac{MF_i \sum_{ex}\sum_{em} I(\lambda_{ex}\lambda_{em})\Delta\lambda_{ex}\Delta\lambda_{em}}{\sum_{i=1}^{5}\varnothing_{i,n}} \times 100\%, i = \text{I-V} \quad (1)$$

where $\varnothing_{i,n}$ is the Ex/Em area volumes referring to the value of region i; $\varnothing_{T,n}$ is the Ex/Em area volumes referring to value of the total region; MF_i is a multiplication factor for each region; $I(\lambda_{ex}\lambda_{em})$ is the fluorescence intensity at each Ex/Em wavelength pair; $\Delta\lambda_{ex}$ and $\Delta\lambda_{em}$ are Ex and Em intervals, respectively. The box charts for FRI analysis were plotted by Origin 9.0 software.

1.4. DFS analysis

The DFS was carried out to distinguish the changes of EEM with various pH values (Eq. (2)).

$$\text{D-EEM}_{pH} = -\frac{1}{l}\left(\frac{\text{EEM}_{pH} - \text{EEM}_{blank-pH}}{C_{pH}} - \frac{\text{EEM}_{pH_{ref}} - \text{EEM}_{blank-pH_{ref}}}{C_{pH_{ref}}}\right) \quad (2)$$

where: D-EEM_{pH} is the differential EEM of FA sub-fraction at certain pH; l is the quartz cell length; EEM_{pH} and EEM_{pHref} are EEM of FA sub-fraction measured at certain and reference pH values, respectively; $\text{EEM}_{blank-pH}$ and $\text{EEM}_{blank-pH_{ref}}$ are EEM of 0.1 mol/L $KClO_4$ measured at various certain pH values, some of which were defined as reference pHs, respectively; C_{pH} and C_{pHref} are concentrations of FA sub-fraction at certain and reference pH values, respectively.

1.5. Discrete Scatchard model

In a heterogeneous mixture of binding sites in sub-fractions of FA (represented by L), the K_{a1} and K_{a2} at acidic and basic pHs, respectively can be defined (Eqs. (3) and (4)) (Appendix A Section S1 and S2).

$$K_{a1} = \frac{[L_1][H]}{[HL_1]} \quad \text{at acidic pH} \quad (3)$$

$$K_{a2} = \frac{K_{ow}[L_2]}{[HL_2][OH]} \quad \text{at basic pH} \quad (4)$$

where $[HL_1]$ (mol/L) and $[HL_2]$ (mol/L) are equilibrium concentrations of binding at acidic pH and basic pH, respectively; $[H]$ (mol/L) is the equilibrium concentration of protons, which were not involved in the main reaction; $[L_1]$ (mol/L) and $[L_2]$ (mol/L) is the equilibrium concentration of ligands which were not involved in the main reaction at acidic pH and basic pH, respectively; C_{L1} (mol/L) and C_{L2} (mol/L) are total concentrations of ligands at acidic pH and basic pH, respectively (Eqs. (5) and (6)).

$$C_{L1} = [L_1] + [HL_1] \quad \text{at acidic pH} \quad (5)$$

$$C_{L2} = [L_2] + [HL_2] \quad \text{at basic pH} \quad (6)$$

The Scatchard function was first applied to estimate stability constants for metal ions binding by proteins (Scatchard, 1949). The Scatchard function was also widely adapted to determine types of binding site for binding of metal ions by humic and fulvic acids (Giesy et al., 1978; Perdue et al., 1984). The Scatchard function is a discrete model which results in a straight line in a Scatchard plot if a single type of binding site present. More than one type of binding site is indicated if the Scatchard plot is curvilinear (Giesy and Alberts, 1989; Giesy and Briese, 1980; Giesy et al., 1986).

In this study, the Scatchard function was interpreted graphically by plotting $V/[H]$ as a function of V at acidic pH and basic pH, respectively (Eqs. (7) and (8)) (Appendix A Fig. S4).

$$V_1 = \frac{[HL_1]}{C_{L1}} \quad \text{at acidic pH} \quad (7)$$

$$V_2 = \frac{[HL_2]}{C_{L2}} \quad \text{at basic pH} \quad (8)$$

In fluorescence titration, it was assumed that FA sub-fraction had consistent fluorescence characteristics and that intensification of fluorescence and concentrations of [HL] were described at acidic pH and basic pH, respectively (Eqs. (9) and (10)).

$$V_1 = \frac{[HL_1]}{C_{L1}} = \frac{F_0 - F}{F_0 - F_{end}} = \frac{\Delta F}{F_0 - F_{end}} \quad \text{at acidic pH} \quad (9)$$

$$V_2 = \frac{[HL_2]}{C_{L2}} = \frac{F_0 - F}{F_0 - F_{end}} = \frac{\Delta F}{F_0 - F_{end}} \quad \text{at basic pH} \quad (10)$$

where F_0 indicated the maximum fluorescence intensity of peaks in EEM recorded at pH 7.0 and normalized by concentration of sub-fractions of FA in the study; F indicated the fluorescence intensity during titration; ΔF represents the fluorescence intensity of peaks in D-EEMs; F_{end} indicated the fluorescence intensity at the end of titration.

1.6. Determination of dissociation constants

In order to quantify the K_a, binding sites during fluorescence titrations, defined here as the fluorescence binding sites of FA sub-fraction, are assumed to have 1:1 stoichiometry between FA sub-fractions and proton. The modified Stern-Volmer equation was used to estimate the K_{a1} and K_{a2} of FA sub-fractions at either acidic or basic pH, respectively

(Berkovic et al., 2012; Esteves da Silva et al., 1998; Yamashita and Jaffé, 2008) (Eq. (11)).

$$\frac{F_0}{\Delta F} = \frac{K_a}{f[H]} + \frac{1}{f} \quad (11)$$

where f represents the fraction of the initial EEM fluorescence that corresponding to the binding fluorophores. Values for f and K_a can be derived by plotting $F_0/\Delta F$ against 1/[H] using SigmaPlot 12.5 software (detailed information of Eq. (11) see Appendix A Section S1 and Section S2).

2. Results and discussion

2.1. FRI analysis of FA sub-fractions at various pHs

Each EEM of five sub-fractions was delineated into five regions (Regions I–V) according to the approach reported previously (Chen et al., 2003). For EEMs of FA_3-FA_{13}, two peaks observed at Ex/Em 290–320/410–445 nm and 250–270/405–440 nm were both located in Region V (Ex/Em 250–450/380–550 nm), which were classified as humic-like (H-L) materials (Fig. S1) (Chen et al., 2002, 2003). For EEMs of FA_3 (pH 7.0–11.5), FA_7 (pH 2.5–11.5), and FA_{13} (9.0–11.5), a peak appeared at Ex/Em 225–240/420–440 nm, which was in Region III (Ex/Em: 200–250/380–550 nm), which was attributed to fulvic-like (F-L) materials (Appendix A Fig. S1) (Chai et al., 2012; Chen et al., 2003; He et al., 2013). Two peaks with shorter Ex were located at Ex/Em of 260–275/310–320 nm and 215–225/300–310 nm, which existed in Region IV (Ex/Em: 250–450/250–380 nm) and Region I (Ex/Em: 200–250/250–330 nm), respectively. These Ex/Em values corresponded to tryptophan-like materials and tyrosine-like materials in FA_9 and FA_{13} (Appendix A Fig. S1) (Chen et al., 2003; He et al., 2013). Region II was related to tyrosine-like materials (Appendix A Fig. S1) (Chen et al., 2003). In this study, tryptophan-like and tyrosine-like materials were assigned to be protein-like materials (Chen et al., 2003; He et al., 2013).

Box charts of distributions of $P_{i,n}$ in FA sub-fractions are shown (Fig. 1). $P_{i,n}$ occurring in Regions I–V were 2.14% ± 2.60%, 2.72% ± 1.43%, 26.4% ± 1.62%, 6.95% ± 3.34%, and 61.80% ± 6.16%, respectively (Fig. 1a). The $P_{III+V,n}$ were more than 80%, showing that F-L and H-L materials were main constituents of all five sub-fractions (Fig. 1a). Mean $P_{i,n}$ and interquartile range have been used previously to compare contents of specific materials in FA sub-fractions (Wei et al., 2016). Mean $P_{I,n}$ and $P_{IV,n}$ of both FA_9 and FA_{13} were greater than those of either FA_3 or FA_5 (Fig. 2b and e), which suggested greater contents of tryptophan-like and tyrosine-like materials in FA_9 and FA_{13}. Mean $P_{III,n}$ and $P_{V,n}$ of both FA_3 and FA_5 were greater than those of FA_7–FA_{13} (Fig. 2b and e), indicating FA_3 and FA_5 contained larger content of F-L and H-L materials than did FA_7–FA_{13}.

FRI distributions over five typical regions of FA sub-fractions at various pHs are shown (Appendix A Fig. S2). Maximum changes of $P_{I,n}$, $P_{II,n}$ and $P_{IV,n}$ that were related to protein-like materials were less than 5%, except for $P_{I,n}$ of FA_9. The $P_{I,n}$ of FA_9 increased from 4.43% to 8.19% in the range of pH 2.5–7.0, then decreased to 1.0% with pH 7.0–11.5 (Appendix A Fig. S2). The $P_{III,n}$ associated with F-L materials of FA_3–FA_{13} was constant in the range of pH 2.5–11.5, where maximum changes of $P_{III,n}$ were less than 5% (Appendix A Fig. S2). Changes in $P_{V,n}$ related to H-L materials were inconsistent for the various sub-fractions of FA. Maximum changes of $P_{V,n}$ were less than 5% for FA_3–FA_7, while maximum changes of $P_{V,n}$ were more than 10% for FA_9 and FA_{13}. $P_{V,n}$ of FA_9 decreased from near 55.0% to about 52.0% in the range of pH of 2.5–7.0, then increased to 65.34% at an range of pH of 7.0–11.5. $P_{V,n}$ of FA_{13} was constant at about 53.0% in the range of pH 2.5–7.0, but increased to 64.53% in the range of pH of 7.0–11.5 (Appendix A Fig. S2). Although pH has a significant effect on intensities of fluorescence of DOM (De Haan et al., 1983; Pace et al., 2012; Yan et al., 2013), it has limited effects on distributions of $P_{i,n}$ of FA sub-fractions. This observation is consistent with those reported previously, where relative proportions of humic and fulvic acids in leachates from landfills were characterized at various stages of stabilization (Chai et al., 2012). Therefore, in this study, DFS was applied to investigate the influence of pH on fluorescence properties of FA sub-fractions.

2.2. DFS analysis of FA sub-fractions with varied pH

The EEM observed at pH 7.0 was used as the reference for each sub-fraction. The D-EEMs of FA sub-fractions at various pHs are shown (Fig. 2). Two main peaks, referred to as Peak A (Ex/Em: 275–320/400–450 nm) and Peak B (Ex/Em: 225–260/400–460 nm), were observed in D-EEMs of FA_3–FA_{13}. Two peaks, including Peak C (Ex/Em: 250–270/300–325 nm) and Peak D (Ex/Em: 200–230/290–310 nm) were also observed in D-EEMs of FA_7–FA_{13}. Based on the FRI regional theory, Peaks A–D were mainly located in Regions V, III, IV and I, respectively (Chen et al., 2003). Therefore, Peaks A–D, which were affected by changes in pH, could then be categorized as H-L, F-L, tryptophan-like, and tyrosine-like materials, respectively (Chen et al., 2003). Under neutral conditions, Peaks A–D were weaker than those under acidic and basic conditions in D-EEMs (Fig. 2).

Effects of changes in pH on ΔF of Peaks A–D for FA sub-fractions are shown (Fig. 3). The ΔF of Peaks A and B decreased from pH 2.5 to 7.0, and increased at pH range of 7.0–11.5 for FA_3–FA_{13} (Fig. 3a and b). ΔF of Peak A decreased in order of $FA_3 > FA_7 > FA_5 > FA_{13} > FA_9$ and $FA_{13} > FA_3 \approx FA_5 > FA_7 > FA_9$ at pH 2.5 and 11.5, respectively. The ΔF of Peak B decreased in order of $FA_3 > FA_7 > FA_{13} \approx FA_5 > FA_9$ and $FA_{13} > FA_3 \approx FA_5 > FA_7 > FA_9$ at pH 2.5 and 11.5, respectively. For Peaks A and B, ΔF exhibited the largest decrease at acidic pH 2.5–5.5 for FA_3, whereas the ΔF exhibited the greatest increase at basic pH 9.0–11.5 for FA_{13} (Fig. 3a and b). Because the hydrolysis processes of carboxylic and phenolic functional groups in DOM were sensitive to pH, the fluorescence intensity of functional groups was also dependent on ionization state conditions (Midorikawa and Tanoue, 1998; Wu and Tanoue, 2001; Yan et al., 2013). According to the previous studies, an acid group, carboxylic-like functionality, in fluorophore of DOM had pKa values between 2.0 and 5.0 (Song et al., 2017; Yan et al., 2013). Additionally, the fluorophore's properties at base conditions were dependent on the phenolic-like functionality, which had the pKa values between 8.0 and 11.0 (Song et al., 2017; Yan et al., 2013). It has been well recognized that carboxylic and phenolic groups overwhelmingly contributed to the changes in fluorescence intensities at pH ranges of 2.0–5.0 and 8.0–11.0, respectively.

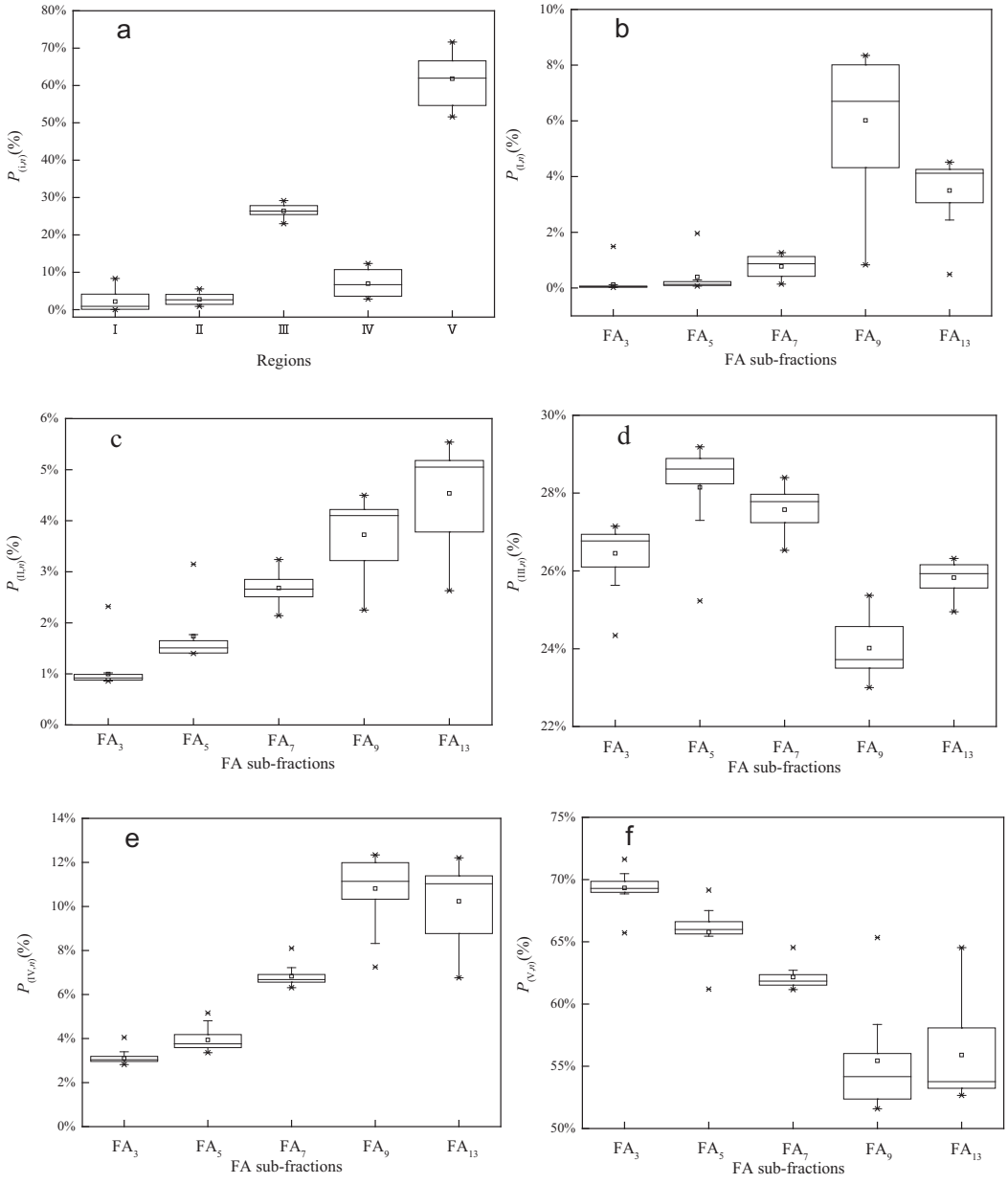

Fig. 1 – Box charts of distributions of $P_{i,n}$ (a), $P_{I,n}$ (b), $P_{II,n}$ (c), $P_{III,n}$ (d), $P_{IV,n}$ (e) and $P_{V,n}$ (f) in excitation-emission matrix spectra of different regions of sub-fractions of fulvic acid.

Based on results discussed above, it was determined that both H-L and F-L materials in FA_3 likely contained more carboxylic groups, and both H-L and F-L materials in FA_{13} likely were composed of more phenolic groups. Additionally, the ΔF of FA_9 produced smaller changes for Peaks A and B than other FA sub-fractions, which indicated less content of both carboxylic and phenolic groups in either H-L or F-L materials in FA_9.

The ΔFs of Peaks C and D of FA_9 were larger than those of FA_7 or FA_{13} under both acidic and basic conditions (Fig. 3c and d). Thus, it was concluded that both tryptophan-like and tyrosine-like materials in FA_9 might contain more carboxylic and phenolic groups than did fractions FA_7 or FA_{13}. The similar ΔFs, which showed decreasing at pH 2.5–5.5, for both Peaks C and D were also observed for fractions FA_7 and FA_{13}. The ΔFs of Peaks C and D of FA_{13} were greater than those of FA_7 at pH 7.5–11.5 (Fig. 3c and d). It is suggested that FA_7 and FA_{13} might be composed of similar amounts of carboxylic groups in both tryptophan-like and tyrosine-like materials, while more phenolic groups were present in both tryptophan-like and tyrosine-like materials in FA_{13}. In addition, intensities of fluorescence of Peaks C and D in D-EEMs of both FA_9 and FA_{13} under basic conditions were larger than those under acidic conditions. This result indicated that mechanisms for quenching of fluorescence for both tryptophan-like and tyrosine-like materials in fractions FA_9 and FA_{13} were more significant under basic conditions (Table 1).

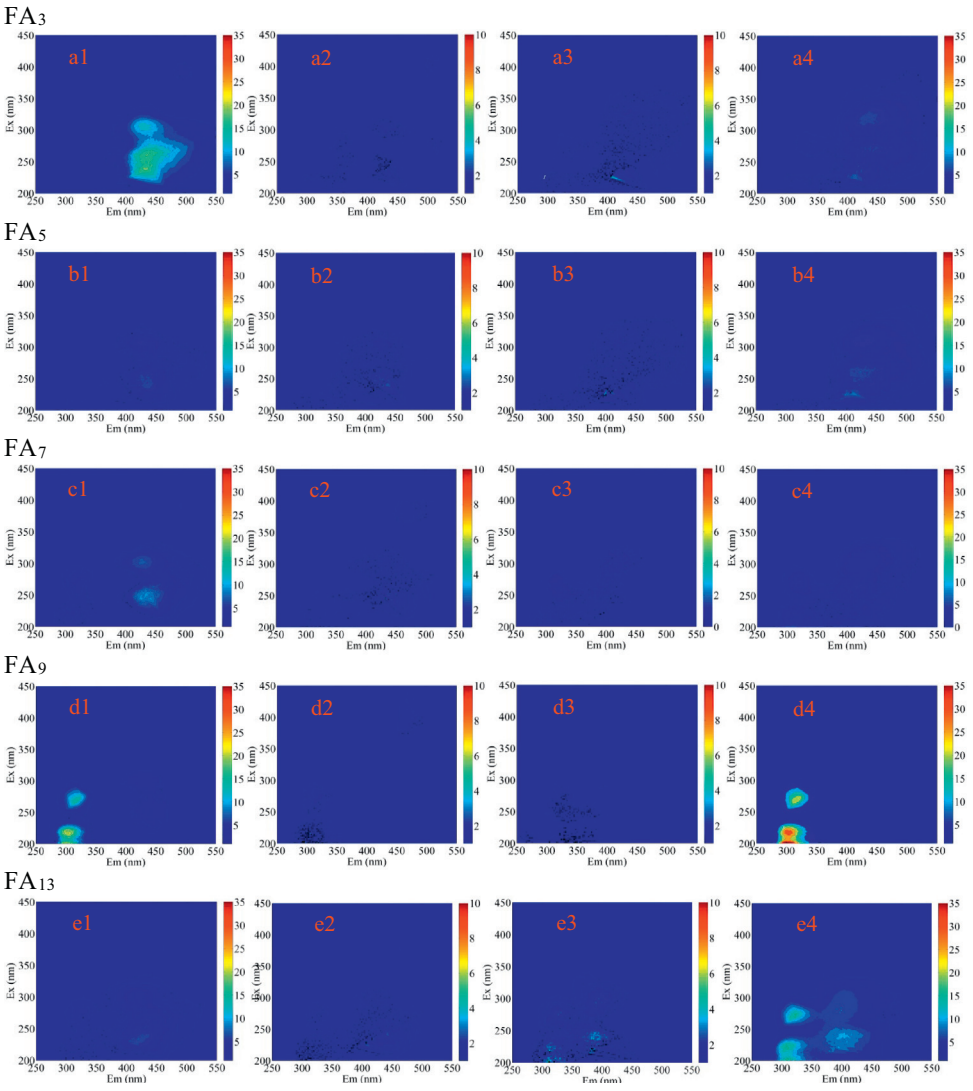

Fig. 2 – Changes in the EEM of sub-fractions of FA at pH 3.0, 5.0, 9.0 or 11.0 with the reference EEM at pH 7.0, respectively: FA_3 (a1–a4); FA_5 (b1–b4); FA_7 (c1–c4); FA_9 (d1–d4); FA_{13} (e1–e4).

2.3. Dissociation constants of FA sub-fractions

To further characterize functional groups responsible for fluorescence peaks in D-EEMs and obtain quantitative information on participation of constituents contributing to peaks in binding of protons, DFS coupled with visualization by use of a modified Stern-Volmer equation, were used to derive pK_as of FA sub-fractions. Parameters for binding of protons, obtained from DFS are shown (Table 2). When fluorescence titration data for binding of constituents in sub-fractions of FA with protons were fitted to the modified Stern-Volmer equation, by use of linear correlations, typical plots of $F_0/\Delta F$ *vs.* $1/[H^+]$ were obtained (Appendix A Fig. S3), which suggested a single mechanism of quenching (Bai et al., 2008). Significant, positive correlations between $F_0/\Delta F$ and reciprocal concentrations of quencher have been reported previously for interactions between DOM and metal ions, such as Cu(II) or Hg(II) (Esteves da Silva et al., 1998; Lu and Jaffe, 2001). The $\log_{10}$ of quenching constants of FA sub-fractions fitted by use of the modified Stern-Volmer equation (R^2 = 0.823–0.998) ranged from 3.12 to 10.99 at pH 2.5–11.5 (Table 2). Based on the diffusion rate of oxygen, the extremely efficient quenchers (10^{10} L/mol/sec), and the typical fluorescence lifetimes (10^{-8} sec) in an aqueous solution, $\log_{10}$ of the dynamic quenching constant cannot exceed 2 at room temperature (25°C) (Bai et al., 2008; Fang et al., 1998). Log_{10} of quenching constants for FA sub-fractions with proton were much greater than that of the extremely efficient quencher (*i.e.* oxygen) (Fang et al., 1998). Therefore, mechanism of static quenching was dominant for interactions between FA sub-fractions and protons. When interactions between protons and DOM from stream waters in Lake Biwa, Japan were investigated, based on pH-dependent fluorescence, static mechanisms of interactions between DOM and protons have been previously suggested (Wu and Tanoue, 2001).

In this study, more than one type of binding site was indicated by the nonlinear Scatchard plot and the discrete, two-component Scatchard function was used to describe

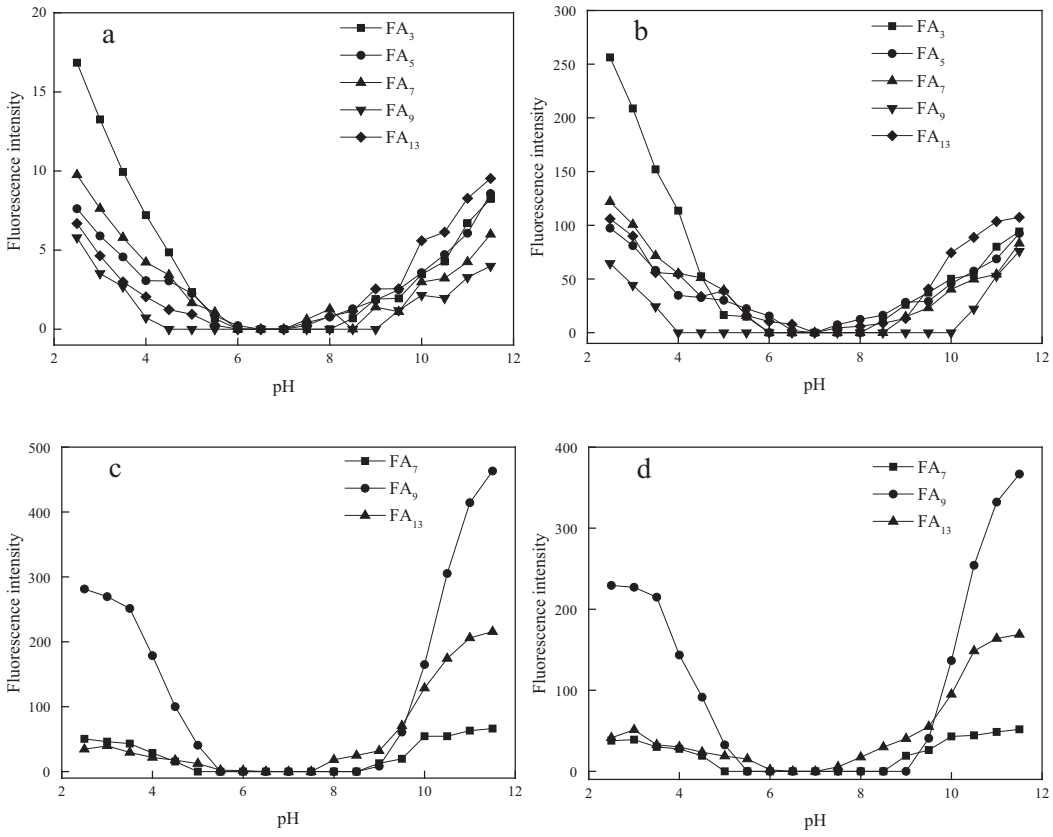

Fig. 3 – Fluorescence intensity of peaks in D-EEMs (ΔF) of sub-fractions of FA (with 10 mg/L) at various pHs (pH_{ref} 7.0): Peak A (a); Peak B (b); Peak C (c); Peak D (d).

binding of protons by sub-fractions of FA (Appendix A Fig. S4). Proton binding by humic acids had been effectively described by a multi-ligand model (Perdue et al., 1984). The nonlinear Scatchard function was also applied for binding metal ions, such as Cu^{2+} by dissolved organic carbon and ultra-filterable material isolated from surface waters (Giesy and Alberts, 1989; Giesy et al., 2010; Giesy and Briese, 1980). The Log_{10} of quenching constants obtained by modified Stern-Volmer equation for acidic and basic pH ranges could be defined as two binding sites, pK_{a1} and pK_{a2} of sub-fractions of FA with ranges from 3.12 to 4.76 and 9.33 to 10.99, respectively (Table 2). The pKa values of carboxylic and phenolic groups of DOM ranged 3.70–4.60 and 8.74–10.31 respectively, by use of potentiometric titrations combined with the modified Henderson-Hasselbalch model (Ritchie and Perdue, 2003). Additionally, pKa values of carboxylic and phenolic groups of

Table 1 – Spectral properties of fluorescence peaks in D-EEMs of five sub-fractions of FA.

Peaks	Sub-fractions	Peak locations (Ex/Em)	Category
Peak A	FA_3	300–310/425–450 nm	Humic-like materials
	FA_5	300–310/410–450 nm	Humic-like materials
	FA_7	290–320/405–450 nm	Humic-like materials
	FA_9	295–305/420–425 nm	Humic-like materials
	FA_{13}	275–300/400–410 nm	Humic-like materials
Peak B	FA_3	225–260/425–450 nm	Fulvic-like materials
	FA_5	225–260/400–450 nm	Fulvic-like materials
	FA_7	225–275/400–460 nm	Fulvic-like materials
	FA_9	240–250/440–450 nm	Fulvic-like materials
	FA_{13}	225–250/400–420 nm	Fulvic-like materials
Peak C	FA_7	260–270/300–310 nm	Tryptophan-like materials
	FA_9	250–270/300–325 nm	Tryptophan-like materials
	FA_{13}	260–270/300–325 nm	Tryptophan-like materials
Peak D	FA_7	200–220/300–310 nm	Tyrosine-like materials
	FA_9	200–230/290–310 nm	Tyrosine-like materials
	FA_{13}	200–220/300–310 nm	Tyrosine-like materials

Table 2 – Proton binding parameters of fluorescence peaks of sub-fractions FA determined by use of the modified Stern-Volmer equation.

Peaks	Sub-fractions	At acidic pH range			At basic pH range		
		pK_{a1}	f	R^2	pK_{a2}	f	R^2
Peak A	FA_3	3.92	0.38	0.955	10.24	0.20	0.943
	FA_5	3.98	0.26	0.867	10.21	0.29	0.910
	FA_7	4.06	0.31	0.908	9.83	0.19	0.891
	FA_9	3.17	0.33	0.955	9.89	0.19	0.968
	FA_{13}	3.48	0.30	0.943	9.71	0.36	0.951
Peak B	FA_3	3.82	0.42	0.980	9.76	0.14	0.882
	FA_5	3.68	0.25	0.908	9.90	0.21	0.903
	FA_7	3.97	0.28	0.823	9.62	0.15	0.970
	FA_9	3.12	0.27	0.998	10.99	0.35	0.994
	FA_{13}	3.75	0.29	0.912	9.77	0.30	0.974
Peak C	FA_7	4.14	0.53	0.994	9.67	0.69	0.943
	FA_9	4.23	0.53	0.998	10.31	0.92	0.998
	FA_{13}	4.45	0.15	0.945	9.84	0.92	0.998
Peak D	FA_7	4.46	0.55	0.910	9.33	0.73	0.956
	FA_9	4.25	0.59	0.992	10.28	0.97	0.996
	FA_{13}	4.76	0.23	0.852	9.81	0.92	0.974

DOM determined by use of spectrophotometric titrations combined with the NICA-Donnan model, ranged 2.66–4.03 and 6.90–8.07 respectively (Dryer et al., 2008; Janot et al., 2010). Values of pK_{a1} for FA sub-fractions were similar to those of DOM from potentiometric titrations and spectrophotometric titrations. However, the pK_{a2} values of FA sub-fractions were similar to those of DOM from potentiometric titrations, and greater than those of DOM determined from spectrophotometric titrations, which might due to the differences in acidity between excited state and ground state of DOM molecule. The fact that data from fluorescence titrations could be fit by use of the two-component Scatchard function does not prove that there were only two distinct binding sites. Rather, it shows that the function with two curve fitting parameters successfully described the average range of values in the mixture. This simplification might be sufficient to describe binding of protons under many circumstances, even though there was a continuous range of strengths of binding sites present.

The pK_{a1}s of Peaks A (3.17–4.06) and B (3.12–3.97) of sub-fractions of FA were comparable, which suggested that H-L and F-L materials had similar affinities for protons. The pK_{a1}s of Peaks A and B were also consistent with those of di-carboxylate molecules (2.5–4.3), indicating that di-carboxylic groups were likely the predominant sites of binding for both H-L and F-L materials with protons at acidic pHs (Smith and Martell, 1989). The pK_{a1} for binding of protons by the first fluorescing ligand of DOM ranged 3.40–4.24, which were similar to those previously reported for sub-fractions of FA (Midorikawa and Tanoue, 1998). The $\log_{10}$ conditional stability constants (log K) of DOM binding of Cu(II), Zn(II) and Hg(II) were 4.7–5.3, 4.24–4.49, and 4.17–4.83, respectively (Hernández et al., 2006; Lu and Jaffe, 2001). The lesser pK_{a1} for H-L and F-L materials and greater log K of Cu(II), Zn(II) and Hg(II) suggested that protons had weaker affinities to H-L and F-L materials than did metal ions. This is expected because divalent metal ions can form ring structures of coordinate covalent bonds that are more stable than bonds that can be formed between monovalent protons and oxygen atoms in F-L or H-L materials (Giesy and Alberts, 1982, 1989). The pK_{a2} of Peak A (9.71–10.24) and Peak B (9.62–10.99) of sub-fractions of FA were similar to those of hydroxyl-benzenes with a range of 8.0–10.0. Thus, phenolic groups might play a key role in proton binding with both H-L and F-L materials of sub-fractions of FA at basic pH.

The pK_{a1}s of Peaks C (4.14–4.45) and D (4.25–4.76) were greater than those of Peaks A or B, which suggested that both tryptophan-like and tyrosine-like materials had greater affinities for protons than did H-L and F-L materials. Using fluorescence quenching titration, $\log_{10}K$ values for Glycyl-L-tryptophan and L-tryptophan with Cu(II) were in the range of 4.88–6.02 (Hays et al., 2004). Based on thermodynamic stability and acid dissociation constants, the first $\log_{10}K$ of L-tyrosine with Cu(II) was 4.77 (Martell and Smith, 1974). These $\log_{10}$ Ks of tryptophan and tyrosine bound to Cu(II) were slightly greater than pK_{a1} values of tyrosine-like and tryptophan-like materials in sub-fractions of FA. These results indicated that the relatively weaker proton binding strengths were present in tryptophan-like and tyrosine-like materials in mixtures of substances comprising sub-fractions of FA. Values for pK_{a2} of Peaks C (9.67–10.31) and D (9.33–10.28) were comparable to pK_a values for amino acids (9.61–12.02) (Aliyu and Na'Aliya, 2009). This observation indicated that amino acid groups in protein-like materials were significant factors during proton binding to sub-fractions of FA at basic pHs. The f values of Peaks A–D were in the range of 0.19–0.38, 0.14–0.42, 0.15–0.92 and 0.23–0.97, respectively (Table 2). Values of f for Peaks C (0.69–0.92) and D (0.73–0.97) for sub-fractions of FA, except for FA_{13} at acidic pHs, were greater than that of Peaks A (0.19–0.29) and B (0.14–0.35). Similar f values were also present during complexation of protein-like material with Cu(II) (0.61–0.76) and Hg(II) (0.76–0.93), respectively (Zhang et al., 2010). The larger f values suggested that a large proportion of organic ligands bound to protons were protein-like materials in sub-fractions of FA (Table 2). The least values of f for Peaks C and D for FA_{13} at acidic pH range need to be further investigated.

3. Conclusions

Based on distributions of percent fluorescence response derived from FRI analysis, H-L and F-L materials, as primary components accounted for more than 80% in five sub-fractions of FA. Tryptophan-like and tyrosine-like materials were present in both FA_9 and FA_{13} compared to FA_3–FA_7. Based on results of DFS analysis, both H-L and F-L materials in FA_3 might contain more carboxylic groups, and more phenolic groups were present in both H-L and F-L materials in FA_{13}. Fewer content of both carboxylic and phenolic groups occurred in all H-L and F-L materials of FA_9. Protein-like materials of FA_9 had more carboxylic and phenolic groups than those of both FA_7 and FA_{13}. Static quenching was the dominant mechanism for the interactions between sub-fractions of F-L materials and proton. Values for pK_{a1} and pK_{a2} for H-L materials of sub-fractions of F-L materials had ranges of 3.17–4.06 and 9.71–10.24, respectively. Simultaneously, pK_{a1} and pK_{a2} for F-L materials exhibited ranges of 3.12–3.97 and 9.62–10.99, respectively. Protonation of both H-L and F-L materials in sub-fractions were associated with di-carboxylate and phenolic functional groups at acidic

and basic pH range. The pK_{a1} for tryptophan-like (4.14–4.45) and tyrosine-like materials (4.25–4.76) were greater than those of H-L and F-L materials, indicating larger affinities to proton for tryptophan-like and tyrosine-like materials in sub-fractions. Values of pK_{a2} for tryptophan-like (9.67–10.31) and tyrosine-like materials (9.33–10.28) were comparable to those of amino acids, which indicated that protonation of protein-like materials was associated with amino acid groups in sub-fractions of FA at basic pH.

Acknowledgments

This work was supported by the National Natural Science Foundation of China (Nos. 41173084, 41521003, 41573130, 41630645, 41703115 and 41503104), the Beijing Natural Science Foundation (No. 8162044), the Canada Research Chair program, Einstein Professor Program of the Chinese Academy of Sciences, and the High Level Foreign Experts Program (#GDT20143200016).

Appendix A. Supplementary data

Supplementary data to this article can be found online at https://doi.org/10.1016/j.jes.2018.02.015.

REFERENCES

Alberts, J.J., Giesy, J., 1983. Conditional Stability Constants of Trace Metals and Naturally Occurring Humic Materials: Application in Equilibrium Models and Verification with Field Data. Aquat. Tert. Humic Material, pp. 333–348.

Aliyu, H.N., Na'Aliya, J., 2009. Determination and stability constants of Manganese (II) amino acid complexes. Bay. J. Pure Appl. Sci. 2, 191–193.

Bai, Y.C., Wu, F.C., Liu, C.Q., Li, W., Guo, J.Y., Fu, P.Q., et al., 2008. Ultraviolet absorbance titration for determining stability constants of humic substances with cu(II) and hg(II). Anal. Chim. Acta 616, 115–121.

Bai, Y., Wu, F., Xing, B., Meng, W., Shi, G., Ma, Y., et al., 2015. Isolation and characterization of Chinese standard fulvic acid sub-fractions separated from forest soil by stepwise elution with pyrophosphate buffer. Sci. Rep. 5, 8723.

Berkovic, A.M., García Einschlag, F.S., Gonzalez, M.C., Pis, D.R., Mártire, D.O., 2012. Evaluation of the Hg^{2+} binding potential of fulvic acids from fluorescence excitation–emission matrices. Photochem. Photobiol. Sci. 12, 384–392.

Chai, X., Liu, G., Zhao, X., Hao, Y., Zhao, Y., 2012. Fluorescence excitation–emission matrix combined with regional integration analysis to characterize the composition and transformation of humic and fulvic acids from landfill at different stabilization stages. Waste Manag. 32, 438–447.

Chen, J., Gu, B., Leboeuf, E.J., Pan, H., Dai, S., 2002. Spectroscopic characterization of the structural and functional properties of natural organic matter fractions. Chemosphere 48, 59–68.

Chen, W., Paul Westerhoff, J.A.L., Booksh, K., 2003. Fluorescence excitation–emission matrix regional integration to quantify spectra for dissolved organic matter. Environ. Sci. Technol. 37, 5701–5710.

De Haan, H., Werlemark, G., De Boer, T., 1983. Effect of pH on molecular weight and size of fulvic acids in drainage water from peaty grassland in NW Netherlands. Plant Soil 75, 63–73.

Dryer, D.J., Korshin, G.V., Fabbricino, M., 2008. In situ examination of the protonation behavior of fulvic acids using differential absorbance spectroscopy. Environ. Sci. Technol. 42 (17), 6644–6649.

Esteves da Silva, J.C.G., Machado, A.A.S.C., Oliveira, C.J.S., Pinto, M. S.S.D.S., 1998. Fluorescence quenching of anthropogenic fulvic acids by Cu(II), Fe(III) and UO_2^{2+}. Talanta 45, 1155–1165.

Fang, F., Kanan, S., Patterson, H.H., Cronan, C.S., 1998. A spectrofluorimetric study of the binding of carbofuran, carbaryl, and aldicarb with dissolved organic matter. Anal. Chim. Acta 373, 139–151.

Giesy, J., 1983. Metal binding capacity of soft, acid, organic-rich waters. Toxicol. Environ. Chem. 6, 203–224.

Giesy, J.P., Alberts, J.J., 1982. Trace Metal Speciation: The Interaction of Metals with Organic Constituent of Surface Waters. pp. 23–24.

Giesy, J.P., Alberts, J.J., 1989. Conditional Stability Constants and Binding Capacities for Copper(II) by Ultrafilterable Material Isolated from six Surface Waters of Wyoming, USA. Springer, Netherlands, pp. 659–680.

Giesy, J.P., Briese, L.A., 1980. Metal binding capacity of northern European surface waters for Cd, Cu, and Pb. Org. Geochem. 2, 57–67.

Giesy, J.P., Briese, L.A., Leversee, G.J., 1978. Metal binding capacity of selected Maine surface waters. Environ. Geol. 2, 257–268.

Giesy, J.P., Geiger, R.A., Kevern, N.R., Alberts, J.J., 1986. UO_2^{2+}-humate interactions in soft, acid, humate-rich waters. J. Environ. Radioact. 4, 39–64.

Giesy, J.P., Alberts, J.J., Evans, D.W., 2010. Conditional stability constants and binding capacities for copper(II) by dissolved organic carbon isolated from surface waters of the southeastern United States. Environ. Toxicol. Chem. 5, 139–154.

Hays, M.D., Ryan, D.K., Pennell, S., 2004. A modified multisite Stern–Volmer equation for the determination of conditional stability constants and ligand concentrations of soil fulvic acid with metal ions. Anal. Chem. 76, 848–854.

He, X.S., Xi, B.D., Wei, Z.M., Jiang, Y.H., Yang, Y., An, D., et al., 2011. Fluorescence excitation–emission matrix spectroscopy with regional integration analysis for characterizing composition and transformation of dissolved organic matter in landfill leachates. J. Hazard. Mater. 190, 293–299.

He, X.S., Xi, B.D., Li, X., Pan, H.W., An, D., Bai, S.G., et al., 2013. Fluorescence excitation–emission matrix spectra coupled with parallel factor and regional integration analysis to characterize organic matter humification. Chemosphere 93, 2208–2215.

He, X.S., Xi, B.D., Gao, R.T., Wang, L., Ma, Y., Cui, D.Y., et al., 2014. Using fluorescence spectroscopy coupled with chemometric analysis to investigate the origin, composition, and dynamics of dissolved organic matter in leachate-polluted groundwater. Environ. Sci. Pollut. Res. 22, 8499–8506.

Hernández, D., Plaza, C., Senesi, N., Polo, A., 2006. Detection of copper(II) and zinc(II) binding to humic acids from pig slurry and amended soils by fluorescence spectroscopy. Environ. Pollut. 143, 212–220.

Janot, N., Reiller, P.E., Korshin, G.V., et al., 2010. Using spectrophotometric titrations to characterize humic acid reactivity at environmental concentrations. Environ. Sci. Technol. 44 (17), 6782–6788.

Lochmueller, C.H., Saavedra, S.S., 1986. Conformational changes in a soil fulvic acid measured by time-dependent fluorescence depolarization. Anal. Chem. 58, 1978–1981.

Lu, X., Jaffe, R., 2001. Interaction between hg(II) and natural dissolved organic matter: a fluorescence spectroscopy based study. Water Res. 35, 1793–1803.

Maqbool, T., Hur, J., 2016. Changes in fluorescent dissolved organic matter upon interaction with anionic surfactant as revealed by EEM-PARAFAC and two dimensional correlation spectroscopy. Chemosphere 161, 190–199.

Martell, A.E., Smith, R.M., 1974. Critical Stability Constants. 6. Plenum Press, pp. 264–283.

Massicotte, P., Frenette, J.J., 2011. Spatial connectivity in a large river system: resolving the sources and fate of disolved organic matter. Ecol. Appl. 21, 2600–2617.
Midorikawa, T., Tanoue, E., 1998. Molecular masses and chromophoric properties of dissolved organic ligands for copper(II) in oceanic water. Mar. Chem. 62, 219–239.
Murphy, K.R., Stedmon, C.A., Graeber, D., Bro, R., 2013. Fluorescence spectroscopy and multi-way techniques. PARAFAC. Anal. Methods 5, 38–65.
Pace, M.L., Reche, I., Cole, J.J., Fernández-Barbero, A., Mazuecos, I. P., Prairie, Y.T., 2012. pH change induces shifts in the size and light absorption of dissolved organic matter. Biogeochemistry 108, 109–118.
Perdue, E.M., Reuter, J.H., Parrish, R.S., 1984. A statistical model of proton binding by humus. Geochim. Cosmochim. Acta 48, 1257–1263.
Ritchie, J.D., Perdue, E.M., 2003. Proton-binding study of standard and reference fulvic acids, humic acids, and natural organic matter. Geochim. Cosmochim. Acta 67, 85–96.
Scatchard, G., 1949. The attractions of proteins for small molecules and ions. Ann. N. Y. Acad. Sci. 51, 660–672.
Smith, R.M., Martell, A.E., 1989. Critical Stability Constants. Amines vol. 2 pp. 1–6.
Song, F., Wu, F., Guo, F., Wang, H., Feng, W., Zhou, M., et al., 2017. Interactions between stepwise-eluted sub-fractions of fulvic acids and protons revealed by fluorescence titration combined with EEM-PARAFAC. Sci. Total Environ. 605-606, 58–65.
Song, F., Wu, F., Xing, B., Li, T., Feng, W., Giesy, J.P., et al., 2018. Protonation-dependent heterogeneity in fluorescent binding sites in sub-fractions of fulvic acid using principle component analysis and two-dimensional correlation spectroscopy. Sci. Total Environ. 616-617, 1279–1287.
Stedmon, C.A., Bro, R., 2008. Characterizing dissolved organic matter fluorescence with parallel factor analysis: a tutorial. Limnol. Oceanogr. Methods 6, 572–579.
Su, B.S., Qu, Z., He, X.S., Song, Y.H., Jia, L.M., 2016. Characterizing the compositional variation of dissolved organic matter over hydrophobicity and polarity using fluorescence spectra combined with principal component analysis and two-dimensional correlation technique. Environ. Sci. Pollut. Res. Int. 23, 9237–9244.
Sun, J., Guo, L., Li, Q., Zhao, Y., Gao, M., She, Z., et al., 2016. Three-dimensional fluorescence excitation–emission matrix (EEM) spectroscopy with regional integration analysis for assessing waste sludge hydrolysis at different pretreated temperatures. Environ. Sci. Pollut. Res. Int. 23, 24061–24067.
Timko, S.A., Gonsior, M., Cooper, W.J., 2015. Influence of pH on fluorescent dissolved organic matter photo-degradation. Water Res. 85, 266–274.
Wang, J., Lü, C., He, J., Zhao, B., 2016. Binding characteristics of Pb^{2+} to natural fulvic acid extracted from the sediments in Lake Wuliangsuhai, Inner Mongolia plateau, P. R. China. Environ. Earth Sci. 75, 1–11.
Wei, Z., Wang, X., Zhao, X., Xi, B., Wei, Y., Zhang, X., et al., 2016. Fluorescence characteristics of molecular weight fractions of dissolved organic matter derived from composts. Int. Biodeterior. Biodegrad. 113, 187–194.
Wu, F., Tanoue, E., 2001. Isolation and partial characterization of dissolved copper-complexing ligands in streamwaters. Environ. Sci. Technol. 35, 3646.
Wu, J., Zhang, H., He, P.J., Shao, L.M., 2011. Insight into the heavy metal binding potential of dissolved organic matter in MSW leachate using EEM quenching combined with PARAFAC analysis. Water Res. 45, 1711–1719.
Wu, H., Zhou, Z., Zhang, Y., Chen, T., Wang, H., Lu, W., 2012. Fluorescence-based rapid assessment of the biological stability of landfilled municipal solid waste. Bioresour. Technol. 110, 174–183.
Wu, F., Bai, Y., Mu, Y., Pan, B., Xing, B., Lin, Y., 2013. Fluorescence quenching of fulvic acids by fullerene in water. Environ. Pollut. 172, 100–107.
Yamashita, Y., Jaffé, R., 2008. Characterizing the interactions between trace, etals and dissolved organic matter using excitation–emission matrix and parallel factor analysis. Environ. Sci. Technol. 42, 7374–7379.
Yan, M., Fu, Q., Li, D., Gao, G., Wang, D., 2013. Study of the pH influence on the optical properties of dissolved organic matter using fluorescence excitation–emission matrix and parallel factor analysis. J. Lumin. 142, 103–109.
Yu, G.H., Luo, Y.H., Wu, M.J., Tang, Z., Liu, D.Y., Yang, X.M., et al., 2010. PARAFAC modeling of fluorescence excitation–emission spectra for rapid assessment of compost maturity. Bioresour. Technol. 101, 8244–8251.
Zhang, D., Pan, X., Mostofa, K.M., Chen, X., Mu, G., Wu, F., et al., 2010. Complexation between Hg(II) and biofilm extracellular polymeric substances: an application of fluorescence spectroscopy. J. Hazard. Mater. 175, 359–365.
Zhou, J., Wang, J.J., Baudon, A., Chow, A.T., 2013. Improved fluorescence excitation-emission matrix regional integration to quantify spectra for fluorescent dissolved organic matter. J. Environ. Qual. 42, 925–930.

Appendix A. Supplementary data

Fluorescence regional integration and differential fluorescence spectroscopy for analysis of structural characteristics and proton binding properties of fulvic acid sub-fractions

Fanhao Song[1], Fengchang Wu[1,*], Weiying Feng[1], Zhi Tang[1], John P. Giesy[1,2], Fei Guo[1], Di Shi[1], Xiaofei Liu[3], Ning Qin[1], Baoshan Xing[4], Yingchen Bai[1,*]

1. State Key Laboratory of Environmental Criteria and Risk Assessment, Chinese Research Academy of Environmental Science, Beijing 10012, China
2. Department of Biomedical and Veterinary Biosciences and Toxicology Centre, University of Saskatchewan, Saskatoon, Saskatchewan, SK S7N 5B3, Canada
3. College of Resources, Environment and Tourism, Capital Normal University, Beijing 100048, China
4. Stockbridge School of Agriculture, University of Massachusetts, Amherst, MA 01003, USA

[*]Corresponding author: E-mails: wufengchang@vip.skleg.cn (Fengchang Wu); yingchenbai@163.com (Yingchen Bai)

Number of Pages (including this cover sheet): 10

Number of Figs.: 4

[*]Corresponding author: Tel.: +86-10-84931804; Fax: +86-10-84931804.

E-mail: wufengchang@vip.skleg.cn; yingchenbai@163.com

Supplementary caption

Fig. S1. Fluorescence regions and excitation-emission wavelength boundaries.

Fig. S2. The pH-dependent FRI distributions over the five typical regions of sub-fractions at various pH: FA_3 (a); FA_5 (b); FA_7 (c); FA_9 (d); FA_{13} (e).

Fig. S3. The representative modified Stern-Volmer plots for Peak A of FA_3 (R^2=0.994) and FA_{13} (R^2=0.993) at pH 2.5-6.5, respectively. The lines represent modified-predicted values.

Fig. S4. Scatchard diagram for Peak A of FA_3. Line b represents values predicted from a two-component Scatchard function.

Section S1 and Section S2 Detailed derivational information of equation (3) in manuscript.

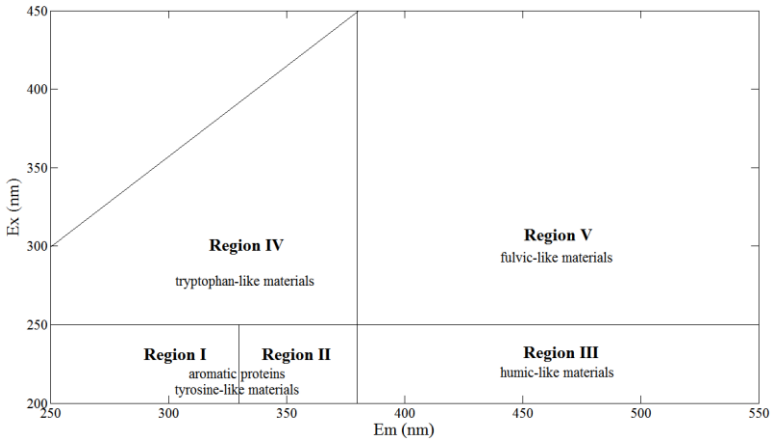

Fig. S1 Fluorescence regions and excitation-emission wavelength boundaries.

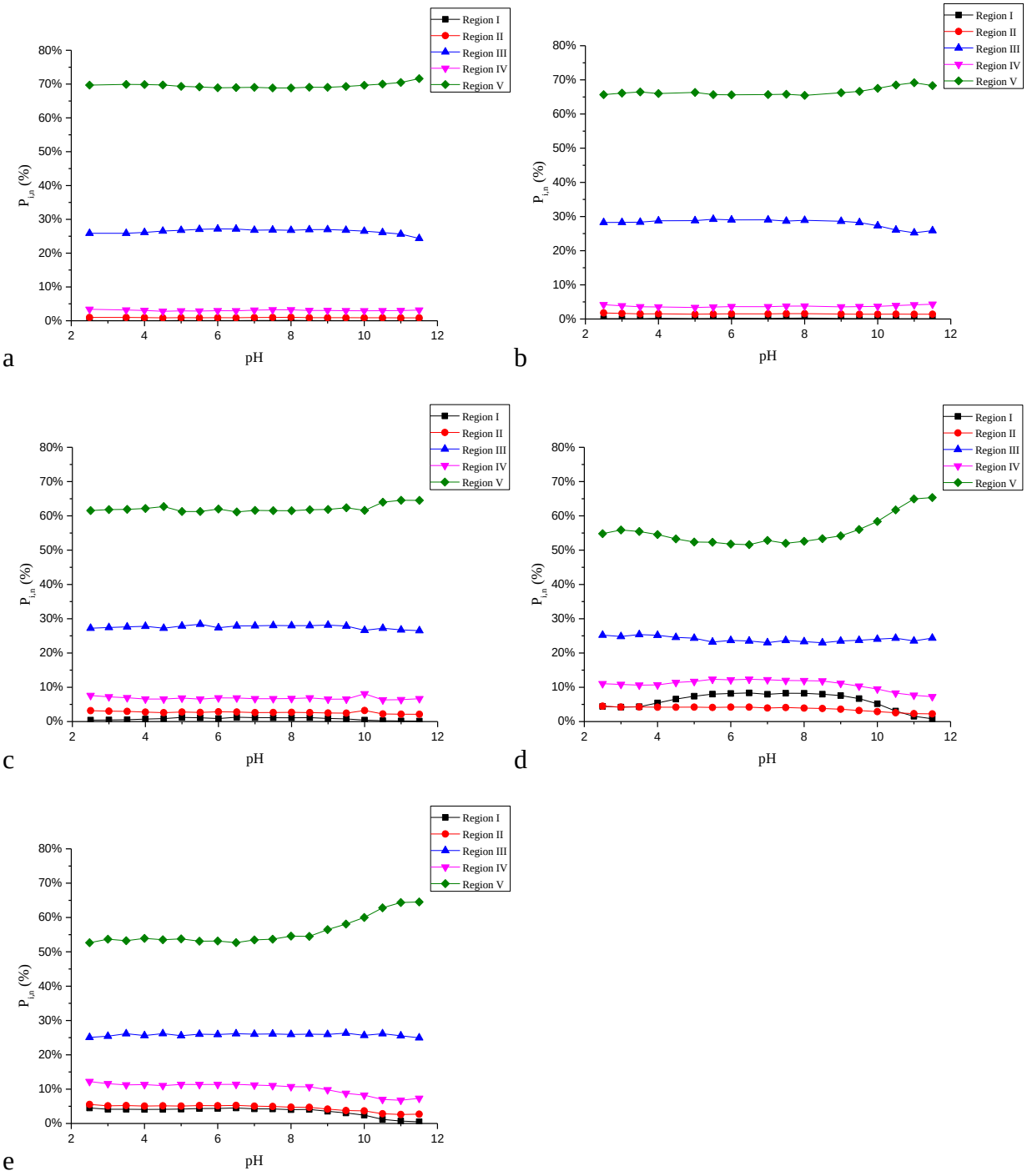

Fig. S2. pH-dependent FRI distributions over the five typical regions of sub-fractions at various pH: FA_3 (a); FA_5 (b); FA_7 (c); FA_9 (d); FA_{13} (e).

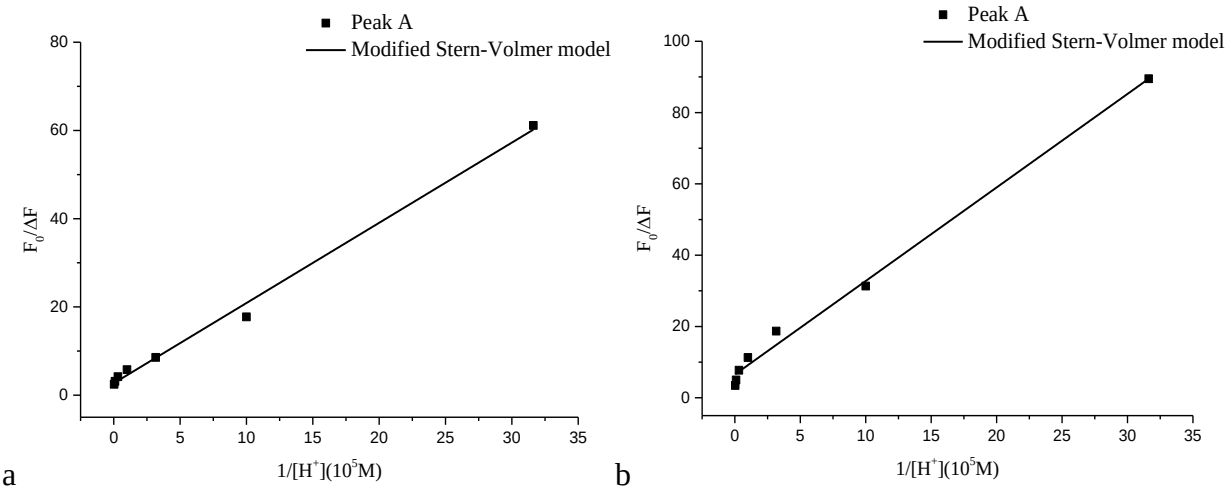

Fig. S3. Representative, modified Stern-Volmer plots for Peak A of FA_3 (R^2=0.994) and FA_{13} (R^2=0.993) at pH 2.5-6.5, respectively. Lines represent modified-predicted values.

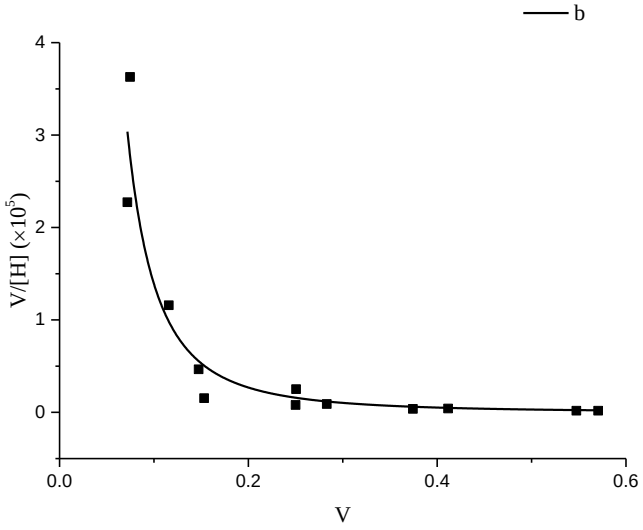

Fig. S4. Scatchard diagram for Peak A of FA_3. Line b represents values predicted from a two-component Scatchard function.

Section S1

Dissociation constants of sub-fractions of FA were estimated from the maximum fluorescence intensity of peaks in D-EEMs at acidic pH range (pH 2.5-6.5). Formation of 1:1 stoichiometry model between the binding sites of sub-fractions of FA (represented by L_1) and proton was assumed at acidic pH range. The proton binding reaction could be expressed (Equation A1)

$$HL_1 \leftrightarrow L_1 + H$$

(A1)

The corresponding dissociation constant, K_{a1}, was (Equation A2).

$$K_{a1} = \frac{[L_1][H]}{[HL_1]}$$

(A2)

where: $[HL_1]$ is the equilibrium concentration of binding process; $[H]$ is the equilibrium concentration of proton which were not involved in the main reaction; $[L_1]$ is the equilibrium concentration of ligands which were not involved in the main reaction; C_{L1} is the total concentration of ligands (Equations A3 and A4).

$$C_{L1}=[L_1]+[HL_1]$$

(A3)

From equation (S2) and (S3):

$$\frac{[HL_1]}{C_{L1}} = \frac{[H]}{K_{a1}+[H]}$$

(A4)

In fluorescence titration, it was assumed that FA sub-fractions molecules had consistent fluorescence characteristics. And the intensification of fluorescence intensity and the concentrations of [*HL*] was described (Equation A5).

$$\frac{[H_{L1}]}{C_{L1}} = \frac{F_0 - F}{F_0 - F_{end}}$$

(A5)

where: F_0 indicated the maximum fluorescence intensity of peaks in EEM recorded at pH 7.0 and normalized by concentration of sub-fractions of FA in the study; F indicated the fluorescence intensity during titration; F_{end} indicated the fluorescence intensity at the end of titration.

From equation (A4) and (A5),

$$\frac{F_0 - F_{end}}{F - F_{end}} = \frac{[H]}{K_{a1}} + 1$$

(A6)

Letting $f = \frac{(F_0 - F_{end})}{F_0}$ in combination with equations (A6) the final relationship was derived (Equation A7).

$$\frac{F_0}{F_0 - F} = \frac{F_0}{\Delta F} = \frac{K_{a1}}{f[\mathrm{H}]} + \frac{1}{f}$$

(A7)

Where: ΔF represents the fluorescence intensity of peaks in D-EEMs at acidic pH range of 2.5-6.5; f represents the fraction of the initial EEM fluorescence that corresponding to the binding fluorophores. f and K_{a1} can be solved by plotting $F_0/\Delta F$ against 1/[H] using SigmaPlot 12.5 software.

Section S2

Dissociation constants of sub-fractions of FA were estimated from the maximum fluorescence intensity of peaks in D-EEMs at acidic pH range (pH 7.5-11.5). Formation of 1:1 stoichiometry model between the binding sites of sub-fractions of FA (represented by L_2) and proton was assumed at acidic pH range. The proton binding reaction was expressed (Equation B1)

$$HL_2 + OH \leftrightarrow L_2 + H_2O$$

(B1)

The conditional stability constant, K_c, and dissociation constant, K_{a2}, can be expressed (Equation B2):

$$K_c = \frac{[L_2]}{[HL_2][OH]} = \frac{K_{a2}}{K_{ow}}$$

(B2)

where: $[HL_2]$ is the equilibrium concentration of binding process; $[L_2]$ is the equilibrium concentration of ligands which were not involved in the main reaction; C_{L2} is the total concentration of ligands. Equations B3 and B4 were derived.

$$C_{L2}=[L_2]+[HL_2]$$

(B3)

From equation (B2) and (B3),

$$\frac{[HL_2]}{C_{L2}} = \frac{K_{ow}}{K_{ow}+K_{a2}[OH]}$$

(B4)

In fluorescence titration, it was assumed that sub-fractions of molecules in FA had consistent fluorescence characteristics. Intensification of fluorescence intensity and the concentrations of [*HL*] was described linearly (Equation B5).

$$\frac{[HL_2]}{C_{L2}} = \frac{F_0 - F}{F_0 - F_{end}}$$

(B5)

where: F_0 indicated the maximum fluorescence intensity of peaks in EEM recorded at pH 7.0 and normalized by concentration of sub-fractions of FA in the study; F indicated the fluorescence intensity during titration; F_{end} indicated the fluorescence intensity at the end of titration.

From equation (B4) and (B5),

$$\frac{F_0 - F_{end}}{F - F_{end}} = \frac{K_{ow}}{K_{a2}[OH]} + 1$$

(B6)

Letting $f = \frac{(F_0 - F_{end})}{F_0}$ in combination with equation (B6), Equation (B7) can be obtained:

$$\frac{F_0}{F_0 - F} = \frac{F_0}{\Delta F} = \frac{K_{a2}}{f[\mathrm{H}]} + \frac{1}{f}$$

(B7)

Where: ΔF represents the fluorescence intensity of peaks in D-EEMs at acidic pH range of 7.5-11.5; f represents the fraction of the initial EEM fluorescence that corresponding to the binding fluorophores. f and K_{a2} can be solved by plotting $F_0/\Delta F$ against 1/[H] using SigmaPlot 12.5 software.